Kinetic Analysis of the Reaction between $(V_2O_5)_{n=1,2}^+$ and Ethylene

Nelly A. Moore,[†] Roland Mitrić,[‡] Dina R. Justes,[†] Vlasta Bonačić-Koutecký,*[,‡] and A. W. Castleman, Jr.*[,†]

Departments of Chemistry and Physics, Pennsylvania State University, University Park, Pennsylvania 16802, and Humboldt Universität zu Berlin, Institut für Chemie, Brook-Taylor-Strasse 2, D-12489 Berlin, Germany

Received: October 4, 2005; In Final Form: December 12, 2005

A systematic experimental and theoretical investigation of the influence of reactant energy on the reactivity of $(V_2O_5)_{n=1,2}^+$ clusters with ethylene (Justes, D. R.; Mitrić, R.; Moore, N. A.; Bonačić-Koutecký, V.; Castleman, A. W., Jr. *J. Am. Chem. Soc*., **2003**, *125*, 6289)[1] provided evidence of the rate controlling steps in the reaction. Herein, we present further experimental and theoretical evidence for our recently proposed radical cation mechanism for oxygen atom transfer from $(V_2O_5)_{n=1,2}^+$ clusters to ethylene. In particular the results of ab initio molecular dynamics simulations are found to further support the radical cation mechanism. Experimental reaction cross sections at the zero pressure limit and rate coefficients show that the energy dependence of the reaction cross section is in accord with the Langevin formula. Evidence is presented that ion−molecule association is the rate determining step, whereas subsequent hydrogen transfer and formation of acetaldehyde proceed without significant barriers. We propose a kinetic model for the reaction cross section that fully accounts for the experimental findings. The model offers the prospect of elucidating the details of the general reaction mechanisms through a study of the energy dependence of the reaction cross sections.

Introduction

There is growing interest in the use of metal oxide clusters as model systems for gaining insight into the mechanisms of various reactions of importance in the field of catalysis.[2−4] Gas-phase cluster research is proving to be very valuable in determining the properties and behavior of transition metal oxides, yielding information on thermochemistry,[5] structure,[6−13] and reactivity.[14−16] Recently, we have undertaken a comprehensive joint theoretical and experimental effort to reveal the reactive behavior of vanadium oxides of various sizes and stoichiometries with a variety of small organic molecules. Our findings show that among vanadium oxides of widely differing stoichiometries and sizes, only $V_2O_5^+$ and $V_4O_{10}^+$ effect oxygen transfer reactions with ethylene.[1,17,18] In particular, these results have prompted us to devote considerable attention to a study of these species. Prior evidence from experimental investigations obtained in our laboratory[1] and theoretical findings revealed evidence of a facile oxygen transfer mechanism in direct analogy to ones believed to occur on vanadia surfaces at reaction sites of similar stoichiometry.[15,18] Our earlier theoretical work, in combination with the experimental studies, proposed the involvement of an oxygen centered radical reaction, proceeding after formation of a metal oxide cluster−molecule complex.[1]

Specifically, we have obtained evidence of a general radical cation mechanism for the oxidation of ethylene on cationic vanadium oxide clusters with the composition $(V_2O_5)_{n=1,2}^+$, leading to the formation of acetaldehyde as a neutral product according to the reactions:[1]

$$V_2O_5^+ + C_2H_4 \rightarrow V_2O_4^+ + C_2H_4O \qquad \text{(I)}$$

$$V_4O_{10}^+ + C_2H_4 \rightarrow V_4O_9^+ + C_2H_4O \qquad \text{(II)}$$

The key point is a radical center located at a peripheral oxygen atom on the $V_2O_5^+$ and $V_4O_{10}^+$ clusters. The reaction is considered to proceed through a generic reaction profile based on energetic data obtained from ab initio calculations as shown in Figure 1. The initial reaction step is believed to proceed via the formation of a complex arising from an ion−molecule collision of A and B (Figure 1). The structural transformation along the reaction pathway indicates that a single bond is ultimately formed between the first carbon atom of the ethylene and the oxygen atom (complex C). This leads to the shift in the radical center, initially located at the oxygen atom, to the second carbon atom of the ethylene molecule. In the second reaction step, a hydrogen atom is transferred from the first to the second carbon atom, forming a complex in which the acetaldehyde molecule is bound to the vanadium atom (complex D). Finally, in the third step, the V−O bond is broken and an acetaldehyde molecule is released, resulting in an overall oxygen transfer process between the two reactants, leading to (E + F).

To provide a more complete understanding of the factors influencing the reaction dynamics of this observed oxygen atom transfer reaction, we have undertaken further experimental and theoretical studies of the energetics of the reaction. The findings, which are reported herein, demonstrate consistency with a proposed mechanism of this reaction that is of considerable interest in the area of fundamental catalysis, as well as in the industrial production of acetaldehyde.[19]

Experimental and Computational Methods

The experiments performed for this study were conducted with a guided ion beam mass spectrometer coupled to a laser vaporization source, described in detail previously[20] and briefly explained here. Metal oxide species were generated by using a laser vaporization source, whereby a vanadium rod was ablated using the second harmonic of a Nd:YAG laser while rotating and translating to continually expose a fresh surface. At a predetermined time, a small amount of oxygen seeded in helium, ∼8%, was pulsed over the surface of the rod, creating a plasma

* Address correspondence to these authors. Phone: (814) 865 7242. Fax: (814) 865 5235. E-mail: awc@psu.edu, vbk@chemie.hu-berlin.de.
[†] Pennsylvania State University.
[‡] Humboldt Universität zu Berlin, Institut für Chemie.

10.1021/jp055652u CCC: $33.50
Published on Web 01/31/2006

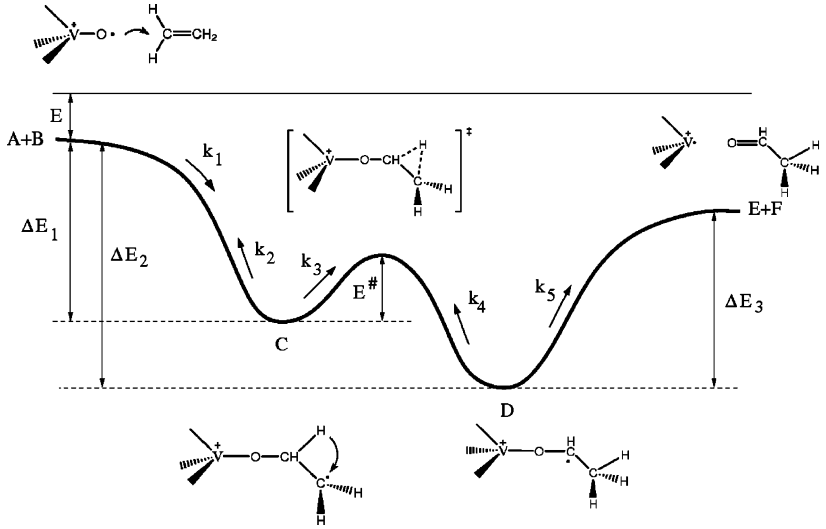

Figure 1. General scheme of the energetic profile and structural transformation of the mechanism for the reaction between $(V_2O_5)_{n=1,2}^+$ and C_2H_4.

in which the vanadium oxide clusters were formed. The clusters were then cooled in a region of supersonic expansion and guided into the first quadrupole through a skimmer and a set of electrostatic lenses. The ion of interest was then mass selected and focused through a second set of electrostatic lenses into a reaction cell incorporated within an octopole guide. The effective path length of the octopole reaction cell was calculated to be 12.9 cm by using the trapezoidal pressure fall-off approximation.[20] The pressure of the ethylene in the reaction cell was kept constant while the energy of the octopole was increased from 0 to 20 V (laboratory frame) in single volt increments. The lab-frame energies (E_{lab}) were converted to center-of-mass frame energy (E_{CM}), $E_{CM} = E_{lab}[M/(M + m)]$, to enable a comparison of calculated and experimental values. Here, M is the mass of the neutral target gas and m is the mass of the selected ion. The described procedure was repeated for pressures ranging from 0.1 to 0.6 mTorr of ethylene, chosen to effect single as well as multiple collision reaction conditions. The products generated in the octopole reaction cell were focused into the second quadrupole through a third set of electrostatic lenses, mass analyzed, and detected with a channel electron multiplier.

The calculations presented here were carried out at the density functional level of theory, using the Becke's hybrid three parameter non-local exchange functional combined with the Lee−Yang−Parr gradient corrected correlation functional (B3LYP)[21] and employing the all-electron triple-ζ valence plus polarization basis set (TZVP) developed by Ahlrichs and co-workers.[22] As shown in our previous work, this method allows for the accurate description of structural properties of cationic vanadium oxide clusters and their interaction with ethylene.[1] The reaction pathways were studied employing ab initio molecular dynamics (MD) with forces calculated by using density functional theory.[23] For the solution of Newton's equations of motion, the Verlet algorithm was used. The MD simulations were initiated from the activated stable complexes of $(V_2O_5)_{n=1,2}^+$ with ethylene by randomly distributing the energy among all degrees of freedom. This allowed us to verify reaction steps deduced from the calculation of the stationary points and obtain support for the proposed mechanism.

Results and Discussion

Ab initio MD simulations at constant energy, corresponding to the stability of the initial complex with respect to the reactants, were carried out to gain further evidence for the operative reaction mechanism. This corresponds to the limiting case of a single collision condition in the experiment[1] in which the energy of the initial complex is not released by collisions with gas molecules.

The snapshots of the MD trajectory for the reaction between $V_2O_5^+$ and C_2H_4 are shown in Figure 2a. The formation of complex C is a barrierless process. The simulation beginning with this complex shows that the association of ethylene to $V_2O_5^+$ is followed by a very rapid (20 fs) hydrogen transfer from the carbon atom bound to oxygen toward the terminal carbon atom. After the hydrogen transfer has taken place (complex D), the V−O bond is broken within the next 40 fs, leading to acetaldehyde and $V_2O_4^+$ as the final products (E and F noted in Figure 1). Analogous snapshots for the reaction between $V_4O_{10}^+$ and C_2H_4 are shown in Figure 2b. Similar to the case of $V_2O_5^+$, the reaction with $V_4O_{10}^+$ also involves very rapid hydrogen transfer (∼30 fs) followed by the formation of acetaldehyde, which occurs typically within 100 fs.

In addition to ab initio MD simulations, experiments were performed by systematically raising the energy of the reaction under conditions of constant selected pressure of ethylene within the reaction cell. Figures 3 and 4 show the branching ratios of the reactions of $V_2O_5^+$ and $V_4O_{10}^+$ with ethylene, respectively. The relative intensities of the ions are plotted as a function of the energy added to the octopole reaction cell. Minor molecular oxygen loss products, $V_2O_3^+$ and $V_4O_8^+$, are observed and are insensitive to the energy addition. The decrease in reactivity with increasing energy is evident from the data in Figure 3, which show that there is comparatively less conversion of $V_2O_5^+$ reactant ion to the major product, $V_2O_4^+$, at higher collision energies. A similar situation arises for $V_4O_{10}^+$ and $V_4O_9^+$ as seen in Figure 4.

In both cases, as the pressure of the ethylene is increased from 0.1 to 0.6 mTorr, the energy under which equal amounts of the parent and the oxygen transfer product ions are attained is increased. This mimics a negative temperature dependence and is not the behavior expected in the case of collision-induced dissociation reactions. In fact, collision-induced dissociation experiments have shown that the observed oxygen deficient products, $V_2O_4^+$ and $V_4O_9^+$, were not the result of a collisional process because they were not observed in separate experiments with an inert gas at near thermal energies.[6] Accordingly, the

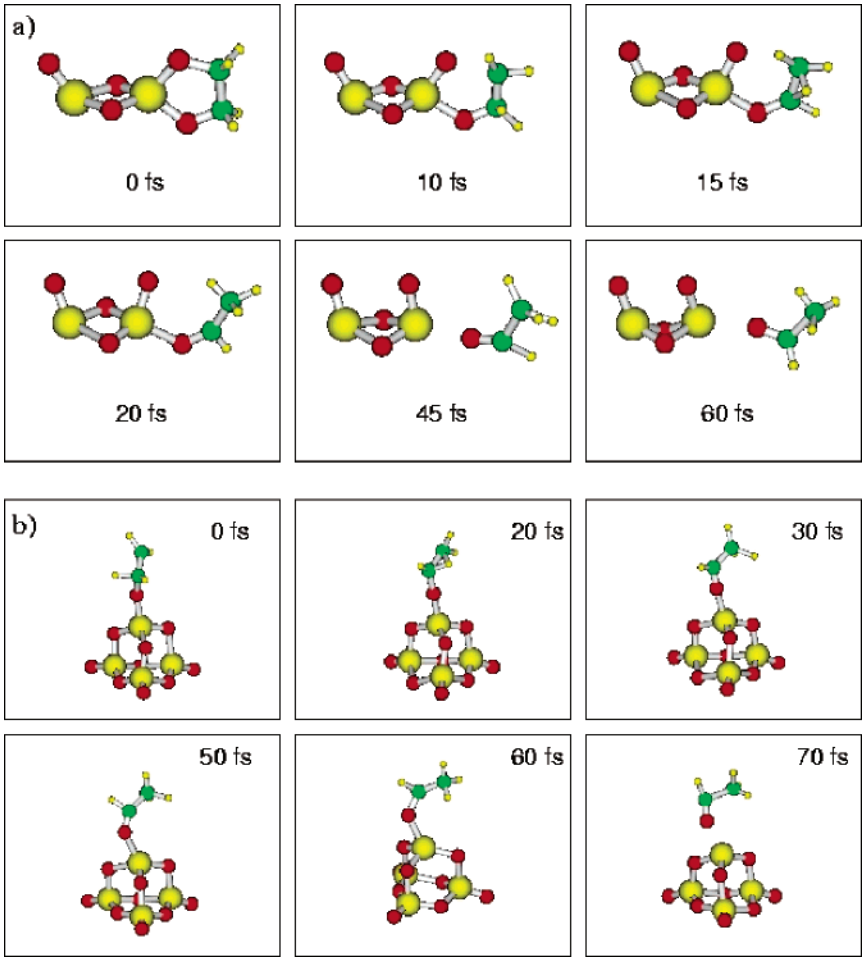

Figure 2. Snapshots of the ab initio MD trajectory calculated by using DFT methods for the reaction of (a) $V_2O_5^+$ with C_2H_4 and (b) $V_4O_{10}^+$ with C_2H_4 leading to the formation of acetaldehyde.

pressure corresponding to the crossing point of the branching ratios can be calculated as follows:

$$I_p = I_0 \exp\left(-\frac{\sigma(E_{CM})pl}{k_B T}\right) \quad (1)$$

where I_0 is the sum of the reactant and all product ion intensities and I_p is the final intensity of the product ion, in this case $V_xO_{y-1}^+$. The total reaction cross section is $\sigma(E_{CM})$ and k_B is the Boltzmann constant. The effective path length of the collision cell is l, while T and p are the temperature and the pressure of the reactant gas, respectively.

Cross Section Anaylsis. The experimental cross sections of both $V_2O_5^+$ and $V_4O_{10}^+$ clusters with ethylene are calculated according to eq 1. To account for the pressure dependence of the cross section measurements, data from several pressures are plotted and then extrapolated to zero pressure in the customary way.[24] At the low-pressure limit, eq 1 becomes

$$\sigma(E_{CM}) = \frac{I_p/I_0}{pl/k_B T} \quad (2)$$

yielding the cross section from the slope of the line in Figure 5 for the intensity ratio I_p/I_0 as a function of pressure. These plots are then repeated for every energy input into the reaction cell.

For $V_4O_{10}^+$, charge transfer and associated ion reaction products, $C_2H_4^+$ and $C_3H_6^+$, can be seen in the branching ratios of Figure 4. These products are accounted for in the cross section

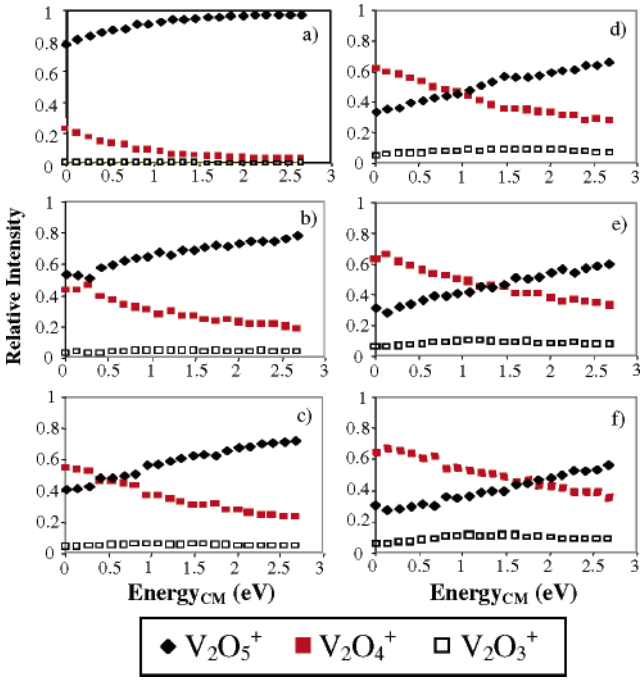

Figure 3. Branching ratios for the energetic analysis of $V_2O_5^+$ with ethylene conducted under the following pressures of ethylene: (a) 0.1, (b) 0.2, (c) 0.3, (d) 0.4, (e) 0.5, and (f) 0.6 mTorr. These are defined by the ratio of each product ion divided by the total ion signal. Notice that the minor contribution of $V_2O_3^+$ is essentially independent of the center-of-mass reaction energy.

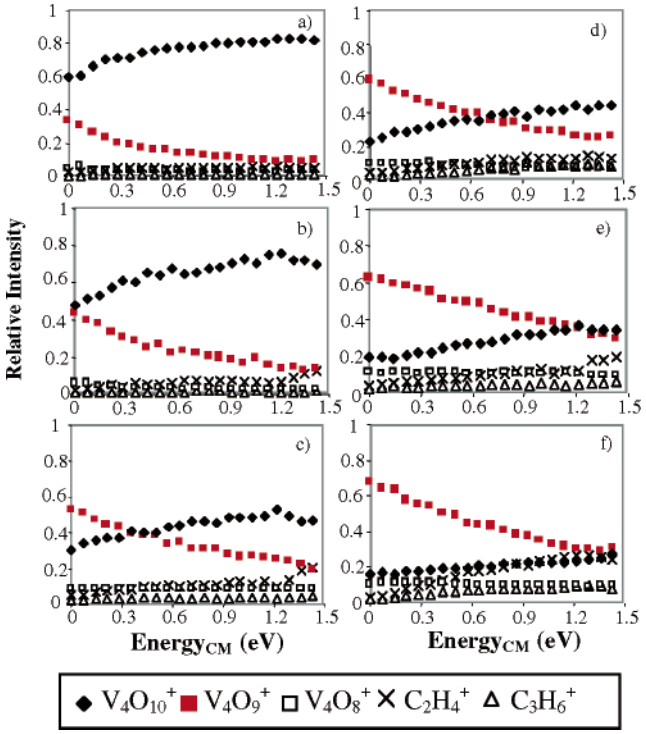

Figure 4. Branching ratios for the energetic analysis of $V_4O_{10}^+$ with ethylene conducted under the following pressures of ethylene: (a) 0.1, (b) 0.2, (c) 0.3, (d) 0.4, (e) 0.5, and (f) 0.6 mTorr.

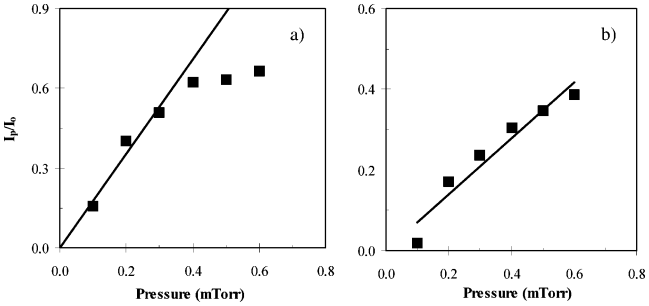

Figure 5. (a) Ratio of product ion intensity, I_p, to total ion intensity, I_0, versus the reaction cell gas pressure for the reaction of $V_2O_5^+$ with ethylene at $E_{CM} = 0$ eV. The equation of the best fit line is $y = 1.77x$ with $R^2 = 0.95$. (b) Ratio of I_p/I_0 versus the reaction cell gas pressure for the reaction of $V_2O_5^+$ with ethylene at $E_{CM} = 2.0$ eV. The equation of the best fit line is $y = 0.697x$ with $R^2 = 0.93$.

calculations through the sum of product intensities via the analysis by using eq 2. The secondary reaction products, which are a consequence of multiple collisions, become significant only at 0.6 mTorr. The experimental cross sections are presented and discussed below with the kinetic model.

Reaction Rates. The reaction rate coefficients, which are dependent on the lifetime of the ion−molecule complex, were also calculated for both oxygen transfer reactions. The experimental cross section data are converted to an expression for the phenomenological rate coefficient[24] by eq 3,

$$k(v_0) = v_0\sigma(E_{CM}) \tag{3}$$

where the relative velocity (v_0) of the reactant ion is

$$v_0 = \left(\frac{2E_{CM}}{\mu}\right)^{1/2} \tag{4}$$

It should be emphasized that this equation is valid only in the case that the energy distribution of the reactant ions is very narrow (monoenergetic ions). The energy input into the reaction cell (E_{CM}) is in the center-of-mass frame, and μ is the reduced mass.

Figure 6 shows the phenomenological rate constants calculated from zero pressure cross section data and therefore does not account for multiple collision conditions in our higher pressure experiments. Another approach to calculate the rate is via the usual method given by eq 5,

$$\frac{dA}{dt} = -k[A][B] \tag{5}$$

and employed in analyzing data acquired in a flow tube reactor operated at low pressures and low electric drift fields. Use of eq 5 requires knowledge of the interaction time in the reaction cell. This time is determined by means of calculation in the present case. The slope of Figure 7, which is a plot of $\ln[I_r/I_0]$ versus the concentration of the reactant gas, is equal to $-kt$. A series of graphs, similar to Figure 7, are plotted for each energy value.

The time is found by estimating the sum of the velocity due to the supersonic nozzle expansion[25] and the velocity acceleration from the voltage field. The supersonic expansion velocity is given by eq 6,

$$v_s = M_T\left[\frac{\gamma RT}{m\left(1 + \frac{\gamma - 1}{2}\right)M_T}\right]^{1/2} \tag{6}$$

where M_T is the mach number, m is the mass of the ion, and γ is the specific heat capacity ratio. In this case, the heat capacity was calculated for atoms because the carrier gas was mostly comprised of helium being pulsed through the nozzle. The velocity due to the voltage applied to the octopole in the reactant gas cell is deduced from eq 7,

$$v = \sqrt{\frac{2qE_{LAB}}{m}} \tag{7}$$

where the charge of the ion is q, and E_{LAB} is the electric field voltage applied to the reaction cell in laboratory frame. The electrostatic lens immediately before the reaction cell is set at 0 V, creating a voltage field difference when energy is added to the octopole. The effective path length of the reaction cell divided by the sum of the velocities provides reaction times ranging from approximately 0.3×10^{-4} to 1×10^{-4} s for $V_2O_5^+$, over the energy range studied, and 0.4×10^{-4} to 1.4×10^{-4} s for $V_4O_{10}^+$. Compared to the effect of the electric field, the contribution due to supersonic expansion is minimal. As the energy in the reaction cell is increased, the time decreases because the ions are moving faster through the cell. These times are within the experimental time frame used in collision-induced dissociation experiments and are due to the short distance between the reaction collision and the quadrupole entrance.[20] Finally, the negative slope of Figure 7 divided by the time corresponding to the energy input yields the rate coefficient.

Figure 8 shows the rate coefficients plotted versus energy. These values were calculated from the experimental data taking into account the product distribution in the case of multiple products. It can be seen from Figure 8 that the rate of $V_2O_5^+$ oxygen transfer is on the order of high-10^{-10} cm^3 s^{-1} and is slightly higher than the rates for $V_4O_{10}^+$ oxygen transfer which are in the mid-10^{-10} cm^3 s^{-1} range. The rate constant for $V_2O_5^+$ at lower energies first increases, and then slowly decreases at

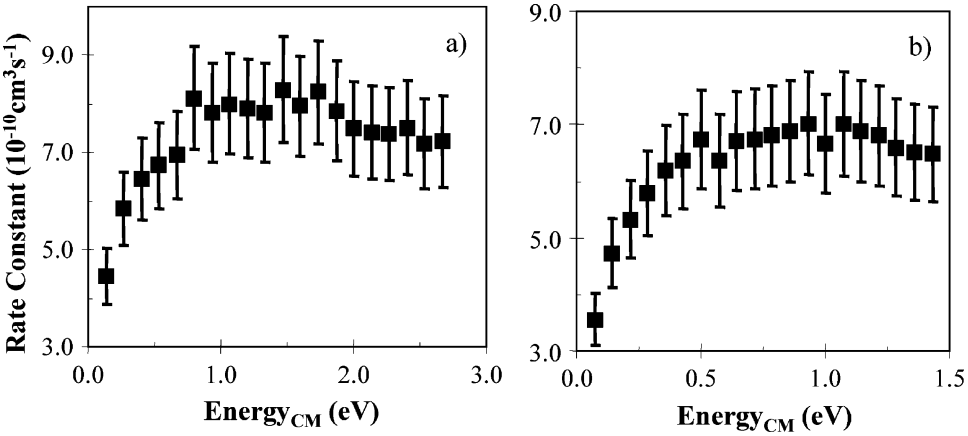

Figure 6. (a) The rate constant versus energy for $V_2O_5^+$ with ethylene calculated from cross section data. (b) The rate constant versus energy for $V_4O_{10}^+$ with ethylene calculated from cross section data. The error bars represent the relative uncertainty in the cross section measurements.

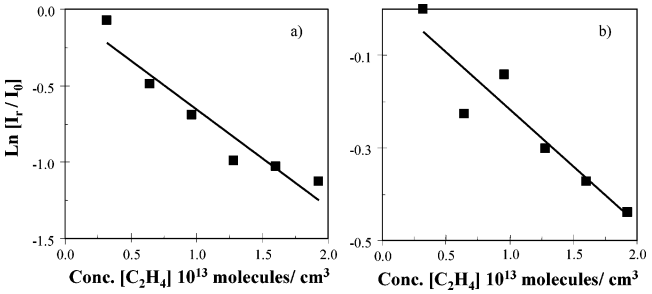

Figure 7. (a) Logarithm of the intensity ratio $[I_r/I_0]$ versus the concentration of C_2H_4 calculated as an ideal gas at $E_{CM} = 0$ eV. The best fit line equation is $y = (-6.41 \times 10^{-14})x - 0.015$ with $R^2 = 0.92$. (b) Logarithm of the intensity ratio $[I_r/I_0]$ versus $[C_2H_4]$ calculated as an ideal gas at $E_{CM} = 2$ eV. The best fit line equation is $y = (-2.48 \times 10^{-14})x + 0.032$ with $R^2 = 0.87$.

values above approximately 1 eV center-of-mass energy. This decrease in the rate constant is expected for an exothermic reaction with negative temperature dependence and no potential barriers. The trend in $V_4O_{10}^+$ is similar with the rate constant increasing and then leveling off at higher energies. It is interesting to note that there is reasonably good agreement in the rate constants derived by the two methods, and presented in Figures 6 and 8, respectively. The data in Figure 6 have been obtained by analyzing data based on single collision conditions to acquire cross sections, and then treated on the basis of a narrow velocity distribution to acquire rate constants. Conversely, the data in Figure 8 are acquired through calculations that describe our experimental conditions of higher pressures in a manner typically employed in flow tube kinetics. Although branching ratios are taken into account, the latter method involves an average rate constant under multiple collision conditions.

Kinetic Model. A kinetic model for the reaction cross section for the oxygen transfer rate follows from eq 1. Combining with eq 3, and as $kt \rightarrow 0$ for short times and low pressure, it follows that

$$\frac{I_r}{I_0} = 1 - \frac{k(\nu_0)p}{k_B T}t \tag{8}$$

where I_r is the intensity of the reactant ion and t is time. This is rearranged in terms of the rate constant and gives eq 9,

$$k(\nu_0) = \frac{I_p/I_0}{(p/k_B T)t} \tag{9}$$

Employing eq 3 and the relationship, $\nu_0 t = l$, along with the crossing points, $I_p/I_0 = 0.5$, shown in Figures 3 and 4, it follows that,

$$p_{1/2} = \frac{k_B T \ln 2}{\sigma(E_{CM})l} \tag{10}$$

and the crossing point for a given energy is a direct measure of the reaction cross section. If we assume that the initial step involves formation of an ion−molecule association between ethylene and the mass selected reactant oxide ion, understanding the reaction cross section requires consideration of the kinetics of several potentially operative reaction steps in the overall conversion mechanism.

To derive the expression for the reaction cross section as a function of energy we write the reaction symbolically in accordance with the mechanism depicted in Figure 1 as

$$A + B \underset{k_2}{\overset{k_1}{\rightleftharpoons}} C \underset{k_4}{\overset{k_3}{\rightleftharpoons}} D \xrightarrow{k_5} E + F \tag{III}$$

By using the steady-state approximation for the intermediates C and D, shown in Figure 1, the change in C and D with respect to time is obtained by the following equations

$$[D] = \frac{k_3[C]}{k_4 + k_5} \tag{11}$$

and

$$[C] = \frac{k_1[A][B]}{k_2 + k_3 - \dfrac{k_3 k_4}{k_4 + k_5}} \tag{12}$$

The individual rate constants shown in the equations are also defined in Figure 1. It readily follows that the total reaction rate d[E]/dt, is given by eq 13

$$\frac{d[E]}{dt} = k_5[D] = \frac{k_1 k_3 k_5}{(k_2 + k_3)(k_4 + k_5) - k_3 k_4}[A][B] \tag{13}$$

and the overall rate constant by eq 14,

$$k = \frac{k_1 k_3 k_5}{(k_2 + k_3)(k_4 + k_5) - k_3 k_4} \tag{14}$$

The first step of the reaction can be modeled after a long-range

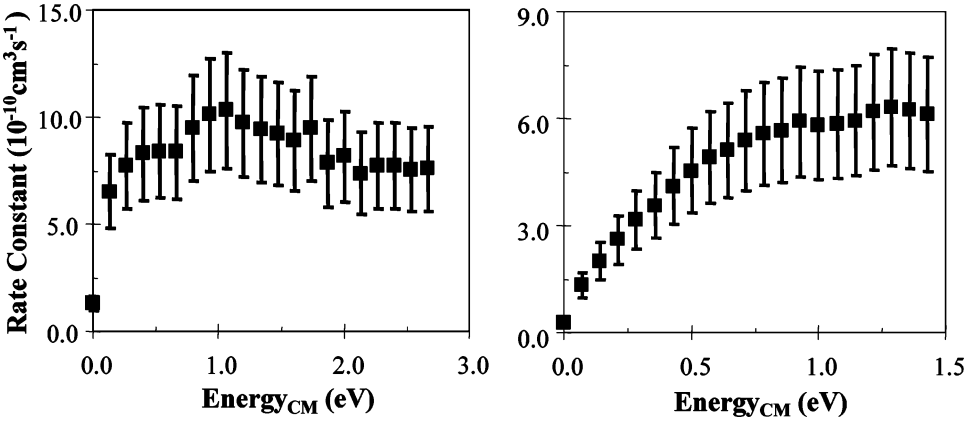

Figure 8. (a) The rate constant versus center-of-mass energy for the reaction of $V_2O_5^+$ with ethylene leading to $V_2O_4^+$ calculated from the velocity of the ions and reaction time and (b) the rate constant versus center-of-mass energy for the reaction of $V_4O_{10}^+$ with ethylene leading to $V_4O_9^+$ calculated from the velocity of the ions and reaction time. The error bars are the relative uncertainties of measurements considered in the calculation.

ion−molecule association, and the reaction cross section can be calculated from the Langevin cross section, σ_L,

$$\sigma_L = \frac{e}{4\epsilon_0}\left(\frac{2\alpha}{E_{CM}}\right)^{1/2} \tag{15}$$

where the collisional energy of the reactant gas is E_{CM}, α is the polarizability of ethylene, and ϵ_0 is the vacuum permittivity. In principle, the rate constants k and k_1 can be obtained from the energy dependent reaction cross sections by averaging over the velocity distribution. However, because the energy distribution of the ions under the considered experimental conditions is narrow, it can be assumed that the velocity distribution is also narrow. In this limiting case, as an approximation, the rate constants k and k_1 are simply products of the velocity of the ions and the corresponding cross sections. This yields a total reaction cross section as

$$\sigma(E_{CM}) = \sigma_L \frac{k_3 k_5}{(k_2 + k_3)(k_4 + k_5) - k_3 k_4} \tag{16}$$

The rate constants for the elementary reaction steps can be approximated by using the RRK expression, yielding the following four equations for k_2, k_3, k_4, and k_5.

$$k_2 = A_2\left(\frac{E}{E + \Delta E_1}\right)^{N-1} \tag{17}$$

$$k_3 = A_3\left(\frac{E + \Delta E_1 - E^{\#}}{E + \Delta E_1}\right)^{N-1} \tag{18}$$

$$k_4 = A_4\left(\frac{E + \Delta E_1 - E^{\#}}{E + \Delta E_2}\right)^{N-1} \tag{19}$$

$$k_5 = A_5\left(\frac{E + \Delta E_2 - \Delta E_3}{E + \Delta E_2}\right)^{N-1} \tag{20}$$

In the above equations, N is taken to be the number of vibrational degrees of freedom. The parameters ΔE_1, ΔE_2, ΔE_3, and $E^{\#}$ are defined in Figure 1 and A_2, A_3, A_4, and A_5 represent the respective frequency factors. The frequency factor A_2 is approximated by the frequency of the normal mode, which leads to the formation of complexes $V_2O_5^+-C_2H_4$ and $V_4O_{10}^+-C_2H_4$ (Figures 2a and 2b, respectively, at $t = 0$). This results in values of $\nu = 992$ cm^{-1} for $V_2O_5^+$ and $\nu = 502.0$ cm^{-1} for $V_4O_{10}^+$. Frequency factors A_3 and A_4 are calculated by using theoretical normal-mode frequencies for the complexes C and D. Complex D is related to the structures shown in Figure 2a ($t = 20$ fs) for $V_2O_5^+-C_2H_4$ and Figure 2b ($t = 50$ fs) for $V_4O_{10}^+-C_2H_4$ and the transition state[1] according to

$$A_{3(4)} = \frac{\Pi_i^N \nu_i}{\Pi_i^{N-1} \nu_i^{\#}} \tag{21}$$

A_5 is approximated by the frequency of the V−O stretching vibration, which leads to the products and has a value of $\nu = 484$ cm^{-1} for $V_2O_5^+-C_2H_4$ and $\nu = 397.3$ cm^{-1} for $V_4O_{10}^+-C_2H_4$ complexes.

To apply RRKM theory to the reaction mechanism given in Figure 1, it is necessary to identify the transition states of the association, hydrogen transfer, and acetaldehyde formation. No transition states are available because the association step engages an ion−molecule reaction without a barrier and the formation of acetaldehyde involves a barrierless V−O bond dissociation. Therefore, RRK theory is used to calculate the rate constants for these two reaction steps, using approximate frequency factors of the normal modes which lead to the association and emanation of acetaldehyde. For the hydrogen transfer step, RRK theory is also used because no low frequency modes are present for which the harmonic approximation underlying RRK theory fails. Moreover, because the barrier for the hydrogen transfer is significantly lower than the total internal energy acquired in the association step, quantitative differences between the RRK and RRKM theory are not expected to influence the final reaction cross section.

Figure 9 compares the experimental cross sections at the zero pressure limit and the cross sections calculated from the Langevin model corresponding to the center-of-mass energy. The theoretical cross sections for the reaction of $V_2O_5^+$ with ethylene in Figure 9a employ eqs 16−20 with the following values for parameters defined in Figure 1: $\Delta E_1 = 3.85$ eV, $\Delta E_2 = 5.19$ eV, $\Delta E_3 = 2.66$ eV, and $E^{\#} = 1.45$ eV obtained from DFT calculations.[1,26] Figure 9b is a plot for the reaction of $V_4O_{10}^+$ and ethylene calculated in the same way with parameter values as follows: $\Delta E_1 = 2.18$ eV, $\Delta E_2 = 4.17$ eV, $\Delta E_3 = 2.16$ eV, and $E^{\#} = 0.13$ eV.[1] As can be seen from eq 16, the total reaction cross section consists of the product of two terms. The first term is the pure Langevin cross section for the association of ethylene with the metal oxide, and the second term is dependent on the rate constants for the subsequent steps (eqs 16−20). The second term involving the rate constants is found through calculations to be unity for these particular

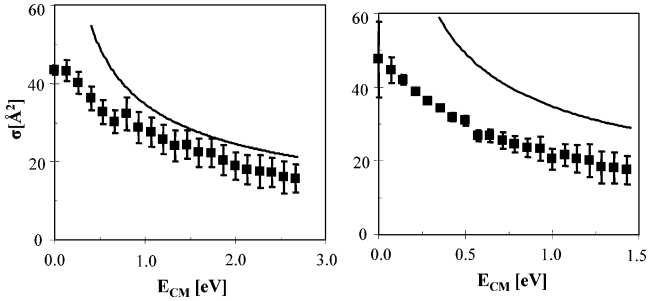

Figure 9. (a) Dependence of the reaction cross sections for $V_2O_5^+$ with ethylene based on the center-of-mass energy for the theoretical model (line) and experimental measurements (squares). (b) Energy dependence of the reaction cross sections for $V_4O_{10}^+$ with ethylene. The error bars represent one standard deviation of the experimental cross section calculated from the root-mean-square value of the least-squares analysis.

parameter values due to the low reaction barriers. Therefore, based on the above assumptions the total reaction cross section is predicted to be accounted for exclusively by the Langevin cross section. It is interesting to note that Hanmura et al. have found that the reaction of benzene with nickel cluster ions is also governed by Langevin kinetics.[27]

Comparing the cross sections obtained theoretically by using eq 16 with those from experiment, we find good agreement between experiment and theory for both systems as shown in Figure 9. It is reasonable that the experimental cross sections are systematically lower, showing that not every collision is an effective collision. Both $V_2O_5^+$ and $V_4O_{10}^+$ with ethylene have decreasing reaction cross sections with increasing energy, characteristic of an exothermic reaction process with a negative temperature dependence.

This provides consistent evidence that subsequent oxygen transfer and formation of acetaldehyde proceed through a mechanism where the barriers are significantly lower than the energy of the initial association complex. On the basis of the theoretical model presented here, together with the experimental findings, we show that the reaction kinetics are comparatively insensitive to the detailed energetics of the involved steps. This applies as long as the barrier for the hydrogen transfer is significantly lower than the energy of the initial complex. This is in contrast to what has been recently claimed for the energy profile differences between the $^2A''$ ground state and the $^2A'$ ground state in $V_2O_5^+$.[9] Although the reaction energies for $V_2O_5^+ + C_2H_4$ change for the $^2A''$ ground state, it is insignificant. The barriers for the reaction are lower in energy than those for the initial rate-limiting association step, showing that the reaction is governed by Langevin kinetics. Hence subsequent reaction steps readily proceed.

Subsequent to the above study, we conducted an investigation to ascertain under which conditions deviations from the Langevin cross sections would be expected to occur. In Figure 10 the reaction cross sections are plotted for four different values of the hydrogen transfer barrier, 1.45, 3.75, 3.85, and 3.88 eV. Whereas the cross section for the situation of a barrier of 1.45 eV is indistinguishable from the Langevin cross sections, deviations start to occur when the barrier reaches a value of 3.85 eV, which corresponds to the energy of the initial complex. For barriers higher than 3.85 eV, the behavior is qualitatively different, giving rise to a cross section that initially increases with energy, reaches a maximum, and then decreases. This is illustrated in Figure 10 for only a slightly increased barrier with respect to 3.85 eV. These findings will allow for insight into

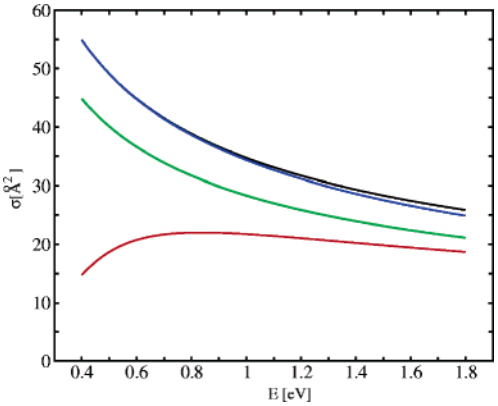

Figure 10. Dependence of the reaction cross section ($\sigma(E_{CM})$) on the center-of-mass energy for different values of the barrier for hydrogen transfer: 1.45 (black line), 3.75 (blue line), 3.85 (green line), and 3.88 eV (red line).

mechanisms of related reactions through a study of the energetics of the reactive cross sections.

Conclusions

A theoretical and experimental analysis of the reaction of $V_2O_5^+$ and $V_4O_{10}^+$ with ethylene provides additional information that demonstrates consistency with the previously proposed energetic profile and mechanism of the oxygen transfer radical cation reaction. Comparison between experimental and theoretical results has given evidence that all steps following the formation of the initial complex as well as the hydrogen transfer reaction proceed with barriers which are significantly lower than that of the initial association complex. This finding supports our earlier proposed reaction mechanism, furthermore showing that the reactions effectively proceed according to the Langevin model. This established that the reaction is driven by the initial rate constant and associated cross section that governs the encounter of the reactants and leads to the formation of an intermediate collision complex. Moreover, the kinetic model proposed allows one, in principle, to estimate the barriers from experimental data on the energy dependence of the reaction cross section, providing important information about cluster reactivity.

Acknowledgment. N.A.M., D.R.J., and A.W.C. gratefully acknowledge the U.S. Department of Energy, Grant No. DE-FG02-92ER14258, for financial support of the experimental work reported herein, and R.M. and V.B.-K. acknowledge support from Deutsche Forschungsgemeinschaft (DFG). We thank Dr. Michele Kimble for helpful discussions during the course of the study.

References and Notes

(1) Justes, D. R.; Mitrić, R.; Moore, N. A.; Bonačić-Koutecký, V.; Castleman, A. W., Jr. *J. Am. Chem. Soc*. **2003**, *125*, 6289.
(2) Muetterties, E. L. *Science* **1977**, *196*, 839.
(3) Fialko, E. F.; Kikhtenko, A. V.; Goncharov, V. B.; Zamaraev, K. I. *J. Phys. Chem. B* **1997**, *101*, 5772.
(4) Waters, T.; O'Hair, R. A. J.; Wedd, A. G. *J. Am. Chem. Soc*. **2003**, *125*, 3384.
(5) Armentrout, P. B. *Int. J. Mass Spectrom*. **2000**, *200*, 219. Xu, J.; Rodgers, M. T.; Griffin, J. B.; Armentrout, P. B. *J. Chem. Phys*. **1998**, *108*, 9339.
(6) Bell, R. C.; Zemski, K. A.; Kerns, K. P.; Deng, H. T.; Castleman, A. W., Jr. *J. Phys. Chem. A* **1998**, *102*, 1733.
(7) Oliveira, M. C.; Marçalo, J.; Vieira, M. C.; Almoster Ferreiraac, M. A. *Int. J. Mass Spectrom*. **1999**, *185*−*187*, 825.
(8) Asmis, K. R.; Brümmer, M.; Kaposta, C.; Santambrogio, G.; von Helden, G.; Meijer, G.; Rademann, K.; Wöste, L. *Phys. Chem. Chem. Phys*. **2002**, *4*, 1101.

(9) Asmis, K. R.; Meijer, G.; Brümmer, M.; Kaposta, C.; Santambrogio, G.; Wöste, L.; Sauer, J. *J. Chem. Phys*. **2004**, *120*, 6461.

(10) Nalewajski, R. F.; Korchowiec, J. *Comput. Chem.* **1995**, *19*, 217.

(11) Pacchioni, G.; Ferrari, A. M.; Giamello, E. *Chem. Phys. Lett*. **1996**, *255*, 58.

(12) Vyboishchikov, S. F.; Sauer, J. *J. Phys. Chem. A* **2000**, *104*, 10913.

(13) Fielicke, A.; Mitrić, R.; Meijer, G.; Bonačić-Koutecký, V.; von Helden, G. *J. Am. Chem. Soc*. **2003**, *125*, 15716.

(14) Kimble, M. L.; Castleman, A. W., Jr.; Mitrić, R.; Bürgel, C.; Bonačić-Koutecký, V. *J. Am. Chem. Soc*. **2004**, *126*, 2526.

(15) Zemski, K. A.; Justes, D. R.; Castleman, A. W., Jr. *J. Phys. Chem. B* **2002**, *106*, 6136.

(16) Berg, C.; Beyer, M.; Achatz, U.; Joos, S.; Niedner-Schatteburg, G.; Bondybey, V. E. *J. Chem. Phys*. **1998**, *108*, 5398.

(17) Justes, D. R.; Mitrić, R.; Bonačić-Koutecký, V.; Castleman, A. W., Jr. *Eur. Phys. J. D* **2003**, *24*, 331.

(18) Zemski, K. A.; Justes, D. R.; Castleman, A. W., Jr. *J. Phys. Chem. A* **2001**, *105*, 10237.

(19) Oyama, S. T.; Middlebrook, A. M.; Somorjai, G. A. *J. Phys. Chem*. **1990**, *94*, 5029.

(20) Bell, R. C.; Zemski, K. A.; Justes, D. R.; Castleman, A. W., Jr. *J. Chem. Phys*. **2001**, *114*, 798.

(21) Becke, A. D. *Phys. Rev. A* **1988**, *98*, 3098. Becke, A. D. *J. Chem. Phys*. **1993**, *98*, 5648. Lee, C.; Yang, W.; Parr, R. G. *Phys. Rev. B* **1998**, *37*, 785.

(22) Schäfer, A.; Horn, H.; Ahlrichs, R. *J. Chem. Phys*. **1994**, *100*, 5829.

(23) Mitrić, R. Ph.D. Thesis, Humboldt University of Berlin, 2003.

(24) Ervin, K. M.; Armentrout, P. B. *J. Chem. Phys.* **1985**, *83*, 166.

(25) Anderson, J. B.; Fenn, J. B. *Phys. Fluids* **1965**, *8*, 780.

(26) Note: $\Delta E_1 = 3.85$ eV has been obtained based on the $^2A'$ ground state of $V_2O_5^+$ (ref 9).

(27) Hanmura, T.; Ichihashi, M.; Kondow, T. *J. Phys. Chem. A* **2002**, *106*, 4525.